Broadband emission processes of Active Galactic Nuclei

Master's Thesis in Physics
Presented by

Andrea Gokus

22.09.2017

Dr. Karl Remeis-Sternwarte Bamberg
Friedrich-Alexander-Universität Erlangen-Nürnberg

Betreuer: Prof. Dr. Jörn Wilms

Abstract

In my Master's Thesis I present two topics related to Active Galactic Nuclei (AGN). These objects are very luminous and emit across the whole electromagnetic spectrum. Radio-loud AGN feature jets, very long and collimated streams of matter, which are observable in all wavelengths as well. The visibility in the radio band is due to synchrotron radiation emitted by electrons. This emission process is the first main topic of this thesis and addressed in detail, covering the complete derivation from the Maxwell equations to the final, self-absorbed spectrum produced by electrons, which follow an energy dependent power-law distribution. As synchrotron radiation is discussed in many publications, but the equations do not always look the same at first sight, an elaborated comparison is conducted.

Numerical methods are necessary for the calculation of a spectrum if the electron distribution does not allow an analytical approximation for the radiation. For power-law distributed electrons one can either determine a numerical or an analytical solution, which is why I use a numeric integrator for the calculation of the spectra first and then compare the results with the analytic approximation of the integrals. Additionally I show problems, which arise from using numeric methods.

The second main topic of this work presents a systematic cross-correlation study of two X-ray satellites, *XMM-Newton* and *NuSTAR*. A good cross-calibration between different instruments is essential for multiwavelength observations, which help understanding astrophysical sources due to analyses in the complete spectral range. For the study, simultaneous observations of AGN are analysed using two different methods. The comparison of the photon indices, which describe the slope of the power-law, allows to detect differences in the calibration of both instruments. By simultaneously fitting both spectra in the overlapping energy band, one can determine the difference in the flux normalisation.

Contents

Chapter 4

Systematic study of simultaneous observations of AGN by *XMM-Newton* and *NuSTAR*

4.1 Introduction

Performing simultaneous observations with different satellites allows us to study energetic sources like X-ray binaries or active galactic nuclei (AGN) in a broader emission regime. As radiation is rarely confined to only a small emission range, we can get better insights in the behaviour of those sources by combining data from all over the spectrum. When studying accreting objects in the X-rays, emission features in the region of the iron K α line (6.4 keV) are important for the analysis of relativistic line broadening near black hole systems. However, good results can only be found when the underlying continuum is well known which requires knowledge about the spectrum in the hard X-rays. Additionally, relativistic reflection effects which range from the lowest energies (1 keV) up to the Compton hump (30 keV) cannot be observed with only one instrument so far. Simultaneous observations in different energy ranges therefore improve the study of energetic sources, variable sources in particular. In order to gain good and reliable results from a simultaneous observation it is necessary to have a very good cross-calibration between the involved satellites. Since a perfect calibration is not possible to achieve, calibration uncertainties introduce discrepancies in the data analysis and impact the determination of astrophysical values. The aim of the work presented in this chapter was to help improving the cross-calibration between *XMM-Newton* and *NuSTAR* by analyzing as many simultaneously performed observations of AGN as there were publicly available at the end of June 2016. This work was a project performed at the European Space Astronomy Center (ESAC) under the supervision of Norbert Schartel and Maria Santos-Lleo.

4.2 The satellites *XMM-Newton* and *NuSTAR*

The X-ray satellite *XMM-Newton* (Jansen et al., 2001) was launched by the European Space Agency (ESA) in 1999. It observes soft X-rays in an energy range from 0.2 to 12 keV with two Reflection Grating Spectrometers (RGSs) and three European Photon Imaging Cameras

(a) *XMM-Newton* ©ESA - D. Ducros (www.esa.int)

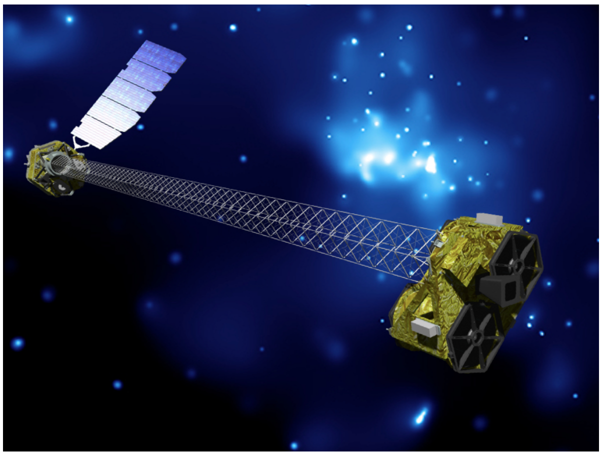

(b) *NuSTAR* ©NASA/JPL-Caltech (www.jpl.nasa.gov)

Figure 4.1: The satellites *XMM-Newton* and *NuSTAR*

(EPICs), namely MOS-1, MOS-2 and PN, which are each at the end of one Wolter type 1 telescope. Additionally, there is an Optical Monitor (OM), a 30 cm mirror telescope, which allows simultaneous observations of an X-ray source in the optical and UV range.
NASA's *Nuclear Spectroscopic Telescope Array* (*NuSTAR*; Harrison et al., 2013) launched in 2012, is the first focusing high-energy instrument in space and observes an energy range from 3 to 79 keV. It has two semiconductor detectors, the Focal Plane Modules A and B (FPMA, FPMB), on which the hard X-rays are focused by using Wolter type 1 approximation optics. Artist's impressions of the satellites in space are shown in Fig. 4.1a and Fig. 4.1b. The main advantage for combining *XMM-Newton* and *NuSTAR* in simultaneous observations is their observational energy overlap between 3 and 12 keV (see Fig. 4.2) which allows for direct comparison of the spacecrafts' calibrations. The instruments of the spacecrafts used in this analysis were the EPIC-pn of *XMM-Newton* and FPMA and FPMB of *NuSTAR*. Since it is necessary to have a good Signal-to-Noise Ratio (S/N) X-ray spectrum, some observations had to be neglected from the available sample. The final data set includes 16 observations from 10 sources (see Table 4.1).

4.3 Data

4.3.1 Extraction

The data was extracted with the standard pipelines. The observations by *XMM-Newton* were extracted using *XMM-Newton* Science Analysis System (SAS) version 15.0.0 aiming to achieve a maximum S/N. Data from the *NuSTAR* spacecraft was extracted using the *NuSTAR* Data Analysis Software (NUSTARDAS) package (v.1.4.1), using nupipeline and the calibration database CALDB20150316 for creating cleaned and calibrated data products. In order to create strictly simultaneous observational data, we used the FTOOL mgtime to merge the gti-files from the observations of both spacecrafts into a common one which was then applied to all observations presented here. All spectra have been binned for a higher S/N ratio. While for the EPIC-pn spectra we used a constant S/N ratio factor of 10 for binning, for the FPM spectra we constantly binned 10 channels together. The complete data set used in this work is given in Table 4.1.

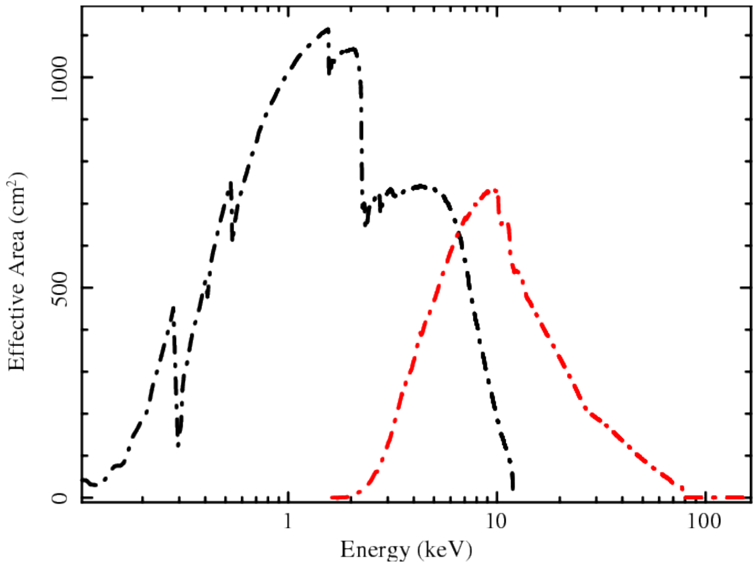

Figure 4.2: Comparison of the effective areas of *XMM-Newton* EPIC-pn camera (black) and *NuSTAR* FPMA (red)

4.3.2 Data Analysis

All spectra were analysed with xspec 12.8.2 using the `wilm` abundances (Wilms et al., 2000) and the `vern` cross sections (Verner et al., 1996). Two different approaches were used to gather information about the differences in the *XMM-Newton* and the *NuSTAR* calibration.
Method 1 includes fitting an EPIC-pn spectrum with a physical model, then applying the model without further change of the parameters to the *NuSTAR* data in order to compare how well the model for the *XMM-Newton* data fits to the *NuSTAR* spectrum.
Method 2 involves simultaneously fitting spectra from EPIC-pn and FPMA/FPMB, respectively, from 3 to 10 keV and retrieving a cross-normalisation constant as well as differences in the power-law indices of the best fit. All errors are 90% confidence unless stated otherwise.

4.3.2.1 Method 1: Comparison of ratios

In Method 1 the ratio of data points to a model are used. The first step is finding a physical, well fitting model for the *XMM-Newton* spectrum. This model is then applied to the *NuSTAR* spectrum without fitting the model again. The comparison of the *NuSTAR* data with the model is done by the ratios, which are directly obtained from xspec.
Whether the observation of a source was used for this method can be seen in the column *Method* of Table 4.1. The applied physical models for each source are given in Table 4.2. Each model contains a power-law (`pegpwrlw` or `bknpower` for a broken power-law). For galactic absorption we used `tbnew_feo`[1] a simple version of the new version of `tbabs` (Wilms et al., 2000). For a source showing relativistic reflection, we applied the `relxill` model (García et al., 2014). `relxill` includes a primary spectrum, which originates in a corona surrounding the accretion disc and is also a power-law, as well as it takes into account the reflection onto the accretion disc. In that way, we can see relativistically broadened emission lines, particularly the iron K α line. In case of the presence of a warm absorber or an extensive soft excess in the spectra, we included the model `warmabs` or a simple blackbody (`bbody`), respectively.

[1] http://pulsar.sternwarte.uni-erlangen.de/wilms/research/tbabs/

Source	Instrument	ObsID	Start Time	End Time	Method
3C 120	EPIC-pn	0693781601	2013-02-06 12:39	2013-02-08 00:51	1, 2
	FPM	60001042002	2013-02-06 12:46	2013-02-06 23:51	1, 2
3C 273	EPIC-pn	0414191001	2012-07-16 11:59	2012-07-16 22:48	1, 2
	FPM	10002020001	2012-07-14 00:06	2012-07-19 23:36	1, 2
Ark 120	EPIC-pn	0693781501	2013-02-18 11:40	2013-02-19 23:54	1, 2
	FPM	60001044002	2013-02-18 10:46	2013-02-20 09:36	1, 2
Centaurus A	EPIC-pn	0724060601	2013-08-07 12:27	2013-08-07 15:47	2
	FPM	60001081002	2013-08-06 13:01	2013-08-07 16:06	2
Fairall 9	EPIC-pn	0741330101	2014-05-09 02:20	2014-05-10 17:37	1, 2
	FPM	60001130002	2014-05-09 02:16	2014-05-09 23:01	1, 2
		60001130003	2014-05-09 23:01	2014-05-11 15:26	1
HE 1136-2304	EPIC-pn	0741260101	2014-07-02 07:44	2014-07-03 14:24	1, 2
	FPM	80002031002	2014-07-02 08:16	2014-07-02 22:31	1, 2
		80002031003	2014-07-02 22:31	2014-07-04 10:01	1, 2
MCG-6-30-15	EPIC-pn	0693781201	2013-01-29 12:08	2013-01-31 01:25	1, 2
	FPM	60001047002	2013-01-29 11:16	2013-01-30 00:11	1, 2
	EPIC-pn	0693781301	2013-01-31 12:01	2013-02-02 01:18	1, 2
	FPM	60001047003	2013-01-30 00:11	2013-02-02 00:41	1, 2
	EPIC-pn	0693781401	2013-02-02 12:02	2013-02-03 01:37	1, 2
	FPM	60001047005	2013-02-02 10:51	2013-02-03 02:41	1, 2
Mrk 915	EPIC-pn	0744490401	2014-12-02 13:08	2014-12-04 02:38	1, 2
	FPM	60002060002	2014-12-02 13:56	2014-12-03 18:46	1, 2
	EPIC-pn	0744490501	2014-12-07 07:46	2014-12-08 03:01	1
	FPM	60002060004	2014-12-07 06:51	2014-12-08 12:46	1
NGC 4593	EPIC-pn	0740920401	2015-01-02 04:46	2015-01-02 11:59	1
	FPM	60001149006	2015-01-02 03:21	2015-01-02 16:36	1
	EPIC-pn	0740920601	2015-01-06 15:01	2015-01-06 23:52	1, 2
	FPM	60001149010	2015-01-06 15:26	2015-01-07 02:31	1, 2
Swift J2127.4+5654	EPIC-pn	0693781701	2012-11-04 17:34	2012-11-06 07:12	1, 2
	FPM	60001110002	2012-11-04 17:21	2012-11-05 18:06	1, 2
		60001110003	2012-11-05 18:06	2012-11-06 08:01	1, 2
	EPIC-pn	0693781801	2012-11-06 17:26	2012-11-08 07:04	1, 2
	FPM	60001110005	2012-11-06 17:56	2012-11-08 07:06	1, 2
	EPIC-pn	0693781901	2012-11-08 17:18	2012-11-09 13:17	1, 2
	FPM	60001110007	2012-11-08 16:51	2012-11-09 13:41	1, 2

Table 4.1: All observations included in the data sample. The spectra were studied using two different methods; the column Method shows whether a source was included in both analysation methods or just one.

As an example, simultaneous spectra from EPIC-pn, FPMA and FPMB are shown in Fig. 4.3 (Ark 120) and Fig. 4.4 (Swift J2127.4+5654). For all models the *NuSTAR* spectra show discrepancies, since the models were fitted to data from the *XMM-Newton* satellite. This approach allows comparing the difference between both spacecrafts indirectly by looking at the ratios. Note that the comparison between EPIC-pn and the FPM detectors does not allow to make a statement about the correlation between the MOS and the FPM detectors. In the ratio plots a slope is visible (e.g. see Fig. 4.3 and Fig. 4.4), causing the FPMA/FPMB values to be higher than the values of EPIC-pn up to 7 keV.

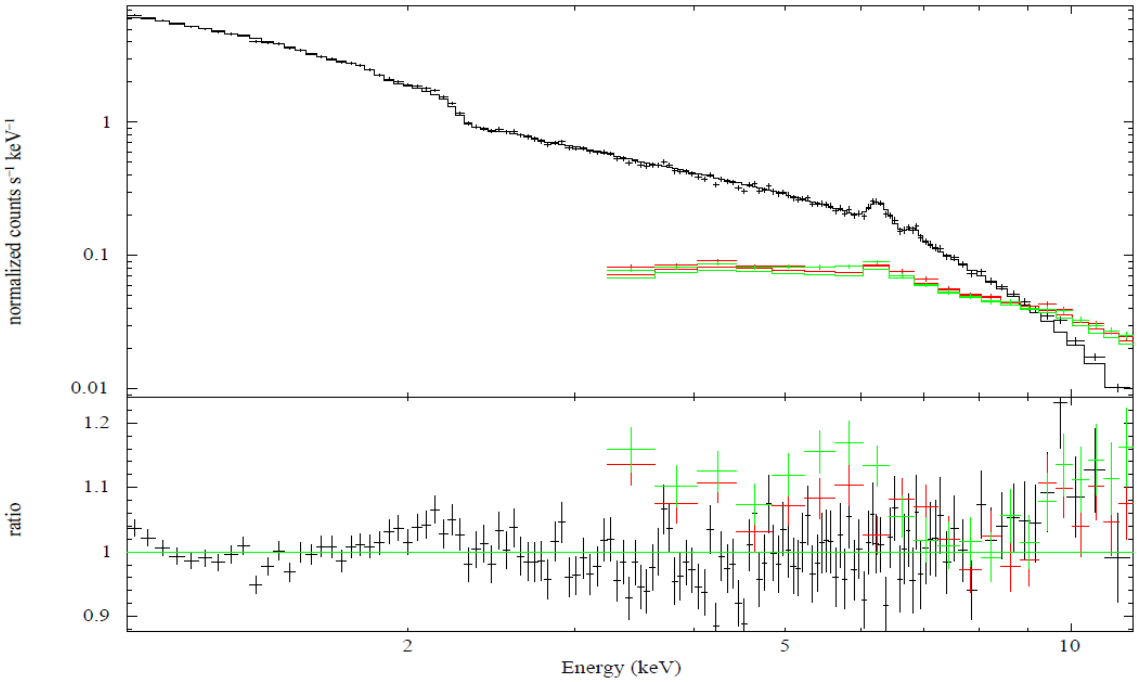

Figure 4.3: Fitted EPIC-pn spectrum (black) of Ark 120 with spectra from both detectors of *NuSTAR* (FPMA: red, FPMB: green) in the upper window. In the lower window ratio values for model vs. data are given for each spectrum.

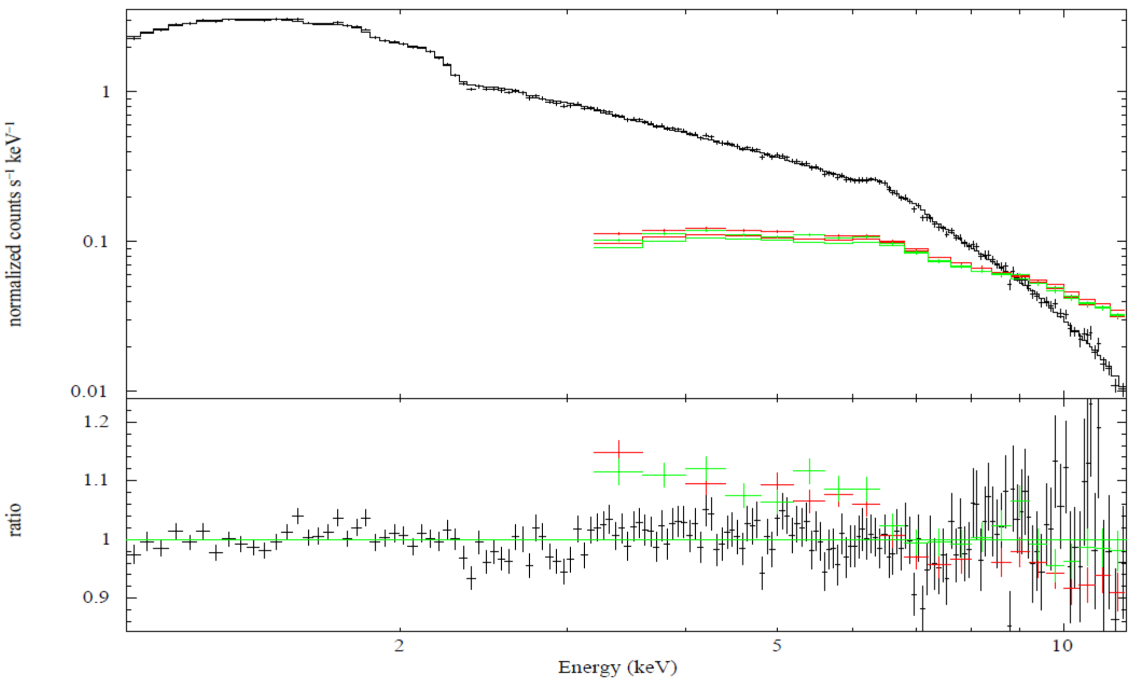

Figure 4.4: Fitted EPIC-pn spectrum (black) of Swift J2127.4+5654 with spectra from both detectors of *NuSTAR* (FPMA: red, FPMB: green) in the upper window. In the lower window ratio values for model vs. data are given for each spectrum.

Source	Model	Reference
3C 120	tbnew_feo×(relxill+zgauss+zgauss)	Lohfink et al. (2013)
3C 273	tbnew_feo×bknpower	Stuhlinger et al. (2004)
Ark 120	tbnew_feo×(bbody+relxill+zgauss+zgauss)	Matt et al. (2014)
Centaurus A	tbnew_feo×(pegpwrlw+zgauss)	Fürst et al. (2016)
Fairall 9	relxill+zgauss	Lohfink et al. (2012)
HE 1136-2304	tbnew_feo×(relxill+zgauss)	Parker et al. (2016)
MCG-6-30-15	tbnew_feo×warmabs(relxill+zgauss)	Wilms et al. (2001)
Mrk 915	warmabs×tbnew_feo×(relxill+zgauss)	Severgnini et al. (2015)
NGC 4593	tbnew_feo×(pegpwrlw+zgauss+zgauss)	Brenneman et al. (2007)
Swift J2127.4+5654	tbnew_feo×(bbody+relxill+zgauss)	Marinucci et al. (2014)

Table 4.2: Models applied on EPIC-pn spectra in Method 1

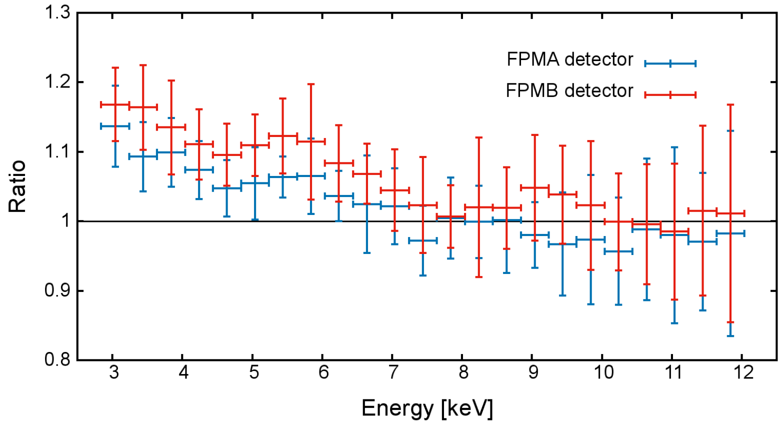

(a) Mean ratio values

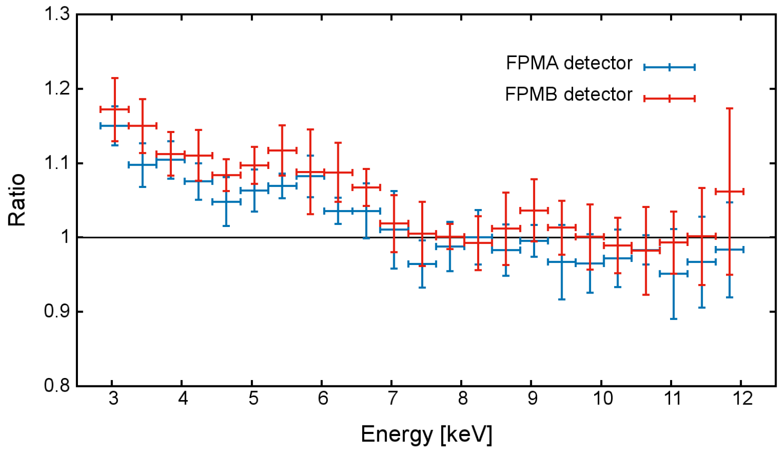

(b) Median ratio values

Figure 4.5: Ratios from FPM spectra compared to best fit to EPIC-pn spectra

In order to get rid of systematics caused by the different models and sources, and to see whether this slope is present in all spectra, we merged all of the ratio plots together in one plot. Figure 4.5a shows the calculated mean values with the according standard deviation, while Fig. 4.5b shows the median with the median absolute deviation. In both plots the ratios unveil deviations between the FPM spectra and the model in the energy range from 3 to 7 keV.

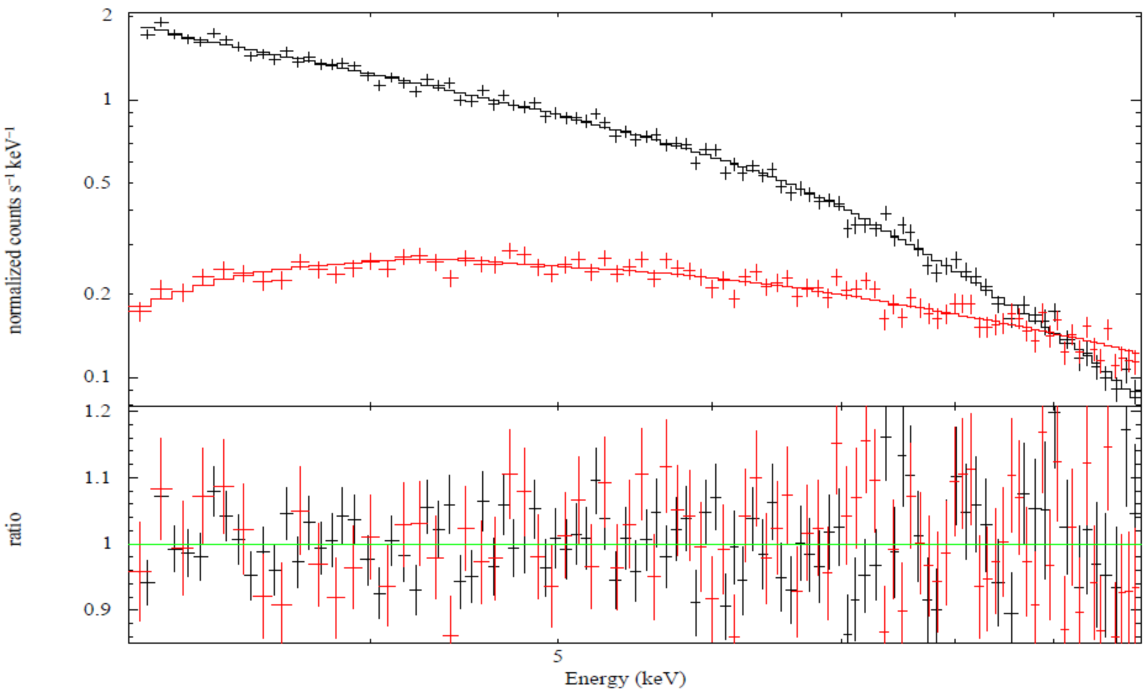

Figure 4.6: Simultaneously fitted EPIC (black) and FPMA (red) spectra of 3C 273. In the lower window the ratio values for model vs. data are given for both fits.

4.3.2.2 Method 2: Simultaneous fitting

Simultaneous fitting in the common energy band can be used to compare different instruments directly. An approach can be adding a cross-normalisation constant to the model, which depicts the difference in flux normalisation. The other way is to compare the photon indices, Γ (the value of the power-law slope), for fitting the same model simultaneously to both spectra and allow only this parameter to vary.
All observations used for this method can be found in the column *Method* of Table 4.1. All fits were done from 3 to 10 keV simultaneously for two detectors each (EPIC-pn & FPMA, EPIC-pn & FPMB) per source. We also fitted the spectra from both FPM detectors simultaneously to check whether there are significant discrepancies between them.
The models used for the sources are shown in Table 4.3. They do not differ much from the models from method 1, but some are kept simpler, because executing the fit in a smaller energy range did not require a blackbody anymore to describe the soft excess which is present below 2 keV. Two example spectra for simultaneous fits are shown in Fig. 4.6 (3C 273) and Fig. 4.7 (MCG–6 – 30 – 15).

The first task is to compare the flux normalisations by using a cross-normalisation constant. A source specific model was fitted to the EPIC-pn spectrum while keeping the same parameters for the FPM spectra (similar to Method 1). In addition to the models shown in Table 4.3 a constant, c, was added and set to 1 for the EPIC-pn spectra, but kept free for the FPM spectra. This cross-normalisation constant represents the difference in the flux normalisations of both instruments. The mean value for this constant is given in Table 4.4). The error was derived through error propagation of the uncertainties determined in the fit. The mean value is fairly close to 1, but a look at the distributions for both FPM detectors (see Fig. 4.8a and Fig. 4.8b) reveals some scattering around the mean value. A difference between the FPM detectors is

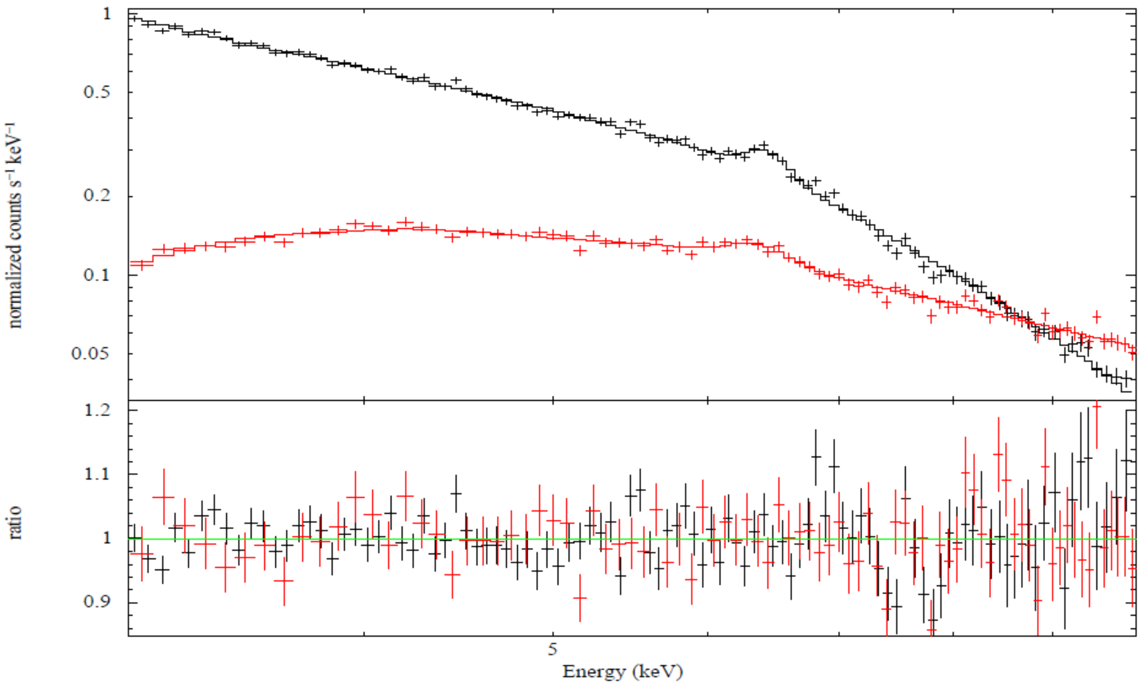

Figure 4.7: Simultaneously fitted EPIC (black) and FPMA (red) spectra of MCG−6 − 30 − 15. In the lower window the ratio values for model vs. data are given for both fits.

Source	Model	Reference
3C 120	tbnew_feox(relxill+zgauss+zgauss)	Lohfink et al. (2013)
3C 273	tbnew_feox×pegpwrlw	Stuhlinger et al. (2004)
Ark 120	tbnew_feox(relxill+zgauss+zgauss)	Matt et al. (2014)
Centaurus A	tbnew_feox(pegpwrlw+zgauss)	Fürst et al. (2016)
Fairall 9	relxill+zgauss	Lohfink et al., 2012
HE 1136-2304	tbnew_feox(relxill+zgauss)	Parker et al. (2016)
MCG-6-30-15	tbnew_feox(relxill+zgauss)	Wilms et al. (2001)
Mrk 915	warmabs×tbnew_feox(relxill+zgauss)	Severgnini et al. (2015)
NGC 4593	tbnew_feox(pegpwrlw+zgauss)	Brenneman et al. (2007)
Swift J2127.4+5654	tbnew_feox(relxill+zgauss)	Marinucci et al. (2014)

Table 4.3: Models applied on EPIC-pn and FPM spectra in Method 2

	c
EPIC-pn/FPMA	1.004 ± 0.034
EPIC-pn/FPMB	1.041 ± 0.034
FPMA/FPMB	1.034 ± 0.019

Table 4.4: Cross-normalisation constants, c, for FPMA and FPMB.

detectable.

Apart from three observations all derived constants lie within the 90% error region for both FPM detectors. The three exceptions are observation 11, 13 and 14 which belong to Centaurus A, Mrk 915 and HE1136-2304 respectively. While obs. 14 is inside the error region accounting its errors, obs. 11 and 13 are definitely off. In the case of Centaurus A, being a close and bright

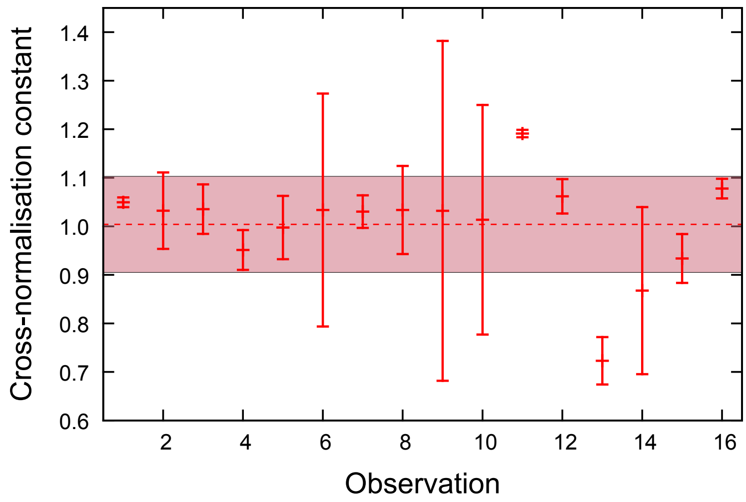

(a) Constants for FPMA.

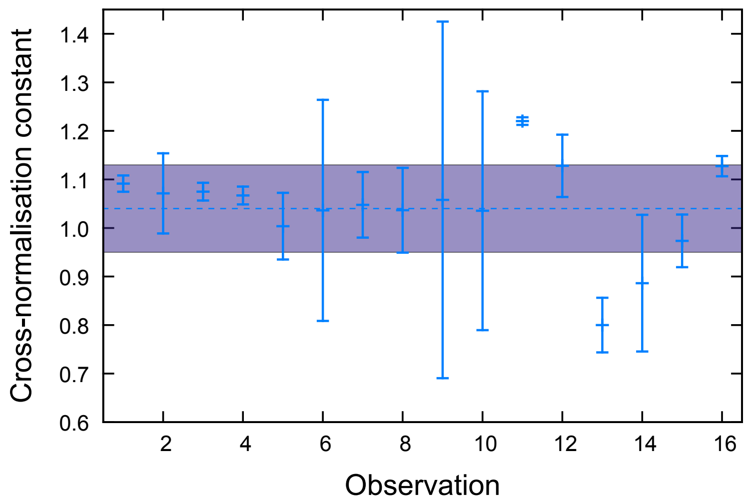

(b) Constants for FPMB.

Figure 4.8: Cross-normalisation constant distributions of FPMA and FPMB for all observations. The dashed line marks the mean value and the 90% error region is coloured.

	c
EPIC-pn/FPMA	1.020 ± 0.017
EPIC-pn/FPMB	1.062 ± 0.018

Table 4.5: Cross-normalisation constants, c, for reduced sample.

source, this offset can be explained with pile up effects being present even though we tried avoiding those in the extraction by excluding the innermost region of the source. For Mrk 915 we have no explanation for the low cross-normalisation in this source. Additionally, observation 6, 9 and 10 have large errors exceeding the 1σ region which makes those results less trustworthy. Excluding these observations (6, 9, 10, 11, 13 and 14), we get larger cross-normalisation constants (see Table 4.5).

Another task was comparing the photon indices for different sources in order to test the

	$\Delta\Gamma$
EPIC-pn-FPMA	0.142 ± 0.025
EPIC-pn-FPMB	0.133 ± 0.025
FPMA-FPMB	0.027 ± 0.004

Table 4.6: Mean values for $\Delta\Gamma$.

	x_0	σ
EPIC-pn/FPMA	0.128 ± 0.006	0.046 ± 0.012
EPIC-pn/FPMB	0.136 ± 0.060	0.112 ± 0.196

Table 4.7: Parameters for a Gaussian fit to the distribution of $\Delta\Gamma$ in a histogram. Note that here, the error σ is just 68% confidence.

calibration of both instruments. For an ideal cross-calibration between both satellites, those values should be the same. In Fig. 4.9 a direct comparison of the photon indices Γ for *XMM-Newton* and *NuSTAR* is shown. We observe a general offset which shows that the FPMA/FPMB spectra have steeper power law slopes than spectra from EPIC-pn. This seems to be present in all observations. In a more direct comparison, Fig. 4.10 presents $\Delta\Gamma$ from 14 observations of 8 sources over flux, showing there is no correlation with flux and therefore no pile-up effects present. The mean differences for EPIC-pn-FPMA, EPIC-pn-FPMB and FPMA-FPMB are shown in Table 4.6. The observation from Centaurus A was excluded from this sample, because it shows a much higher discrepancy between the slopes in *XMM-Newton* and *NuSTAR* data which might be due to pile up. Note that $\Delta\Gamma$ is much smaller for the comparison between both FPM detectors than between the two satellites.

Another way to look at the results is via a distribution in a histogram. The difference $\Delta\Gamma$ is shown for all 16 observations in Fig. 4.11a and Fig. 4.12a. For both histograms we used a bin size of $\Delta\Gamma = 0.01$ in order to get a clearer overview of the distribution. Since the value at $\Delta\Gamma = 0.4$ (from spectra of Centaurus A) is clearly aside the other results and was already excluded in the calculation of the mean $\Delta\Gamma$ (see Table 4.6), we ignored it. Figure 4.11b shows the remaining columns. In order to look at the normal distribution fitted to that data, we excluded also the two observations which had $\Delta\Gamma > 0.2$ (Mrk 915 and NGC 4593). The remaining data was fitted by a normal distribution of $f(x) = A \cdot \exp(-((x - x_0)/\sigma)^2)$. The same was done for the FPMB detector (see Fig. 4.12). Values with $\Delta\Gamma > 0.2$ were excluded again, which concerned again the observation of Centaurus A.

The parameters x_0 and σ of the Gaussian fit are shown in Table 4.7 for both histograms. Note that here, σ is only a 68% confidence error. While the fit delivers good results for the comparison of EPIC-pn and FPMA, it is more problematic in case of the EPIC-pn-FPMB comparison. There the uncertainties on both parameters are too large to give reasonable constraints, because the values are more spread than in the comparison with FPMA. Over all we find very similar results for the histogram approach as in Table 4.6. The difference of the photon index Γ between the EPIC-pn and FPM spectra indicates a principal, energy dependent mis-calibration in either, or in both of the two instruments.

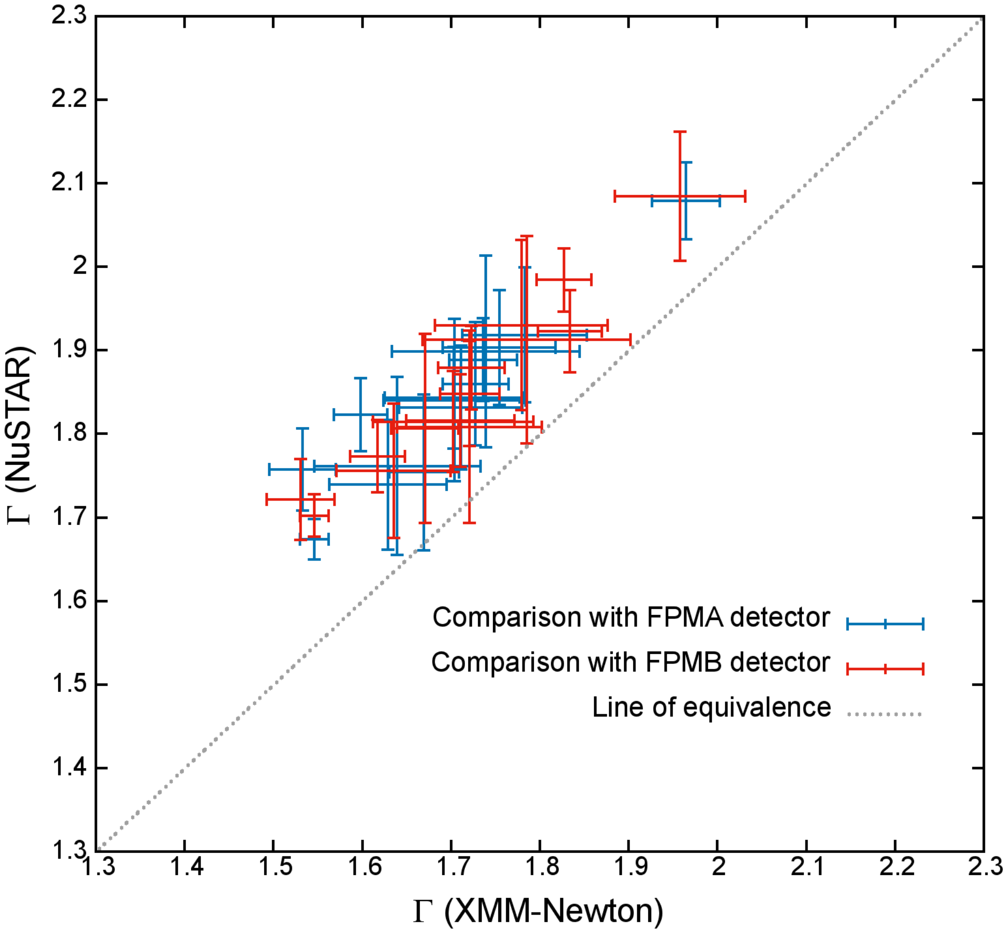

Figure 4.9: Direct comparison of photon indices Γ for *XMM-Newton* and *NuSTAR*. The ideal case would be that the data points are on the line of equivalence which is not observed.

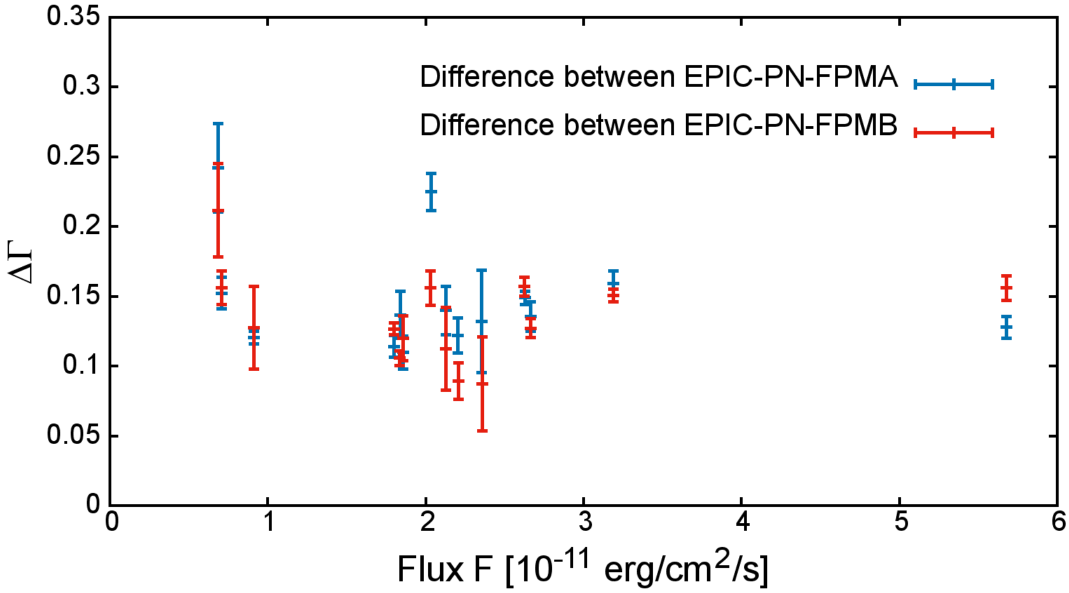

Figure 4.10: Individual ΔΓ over flux of source.

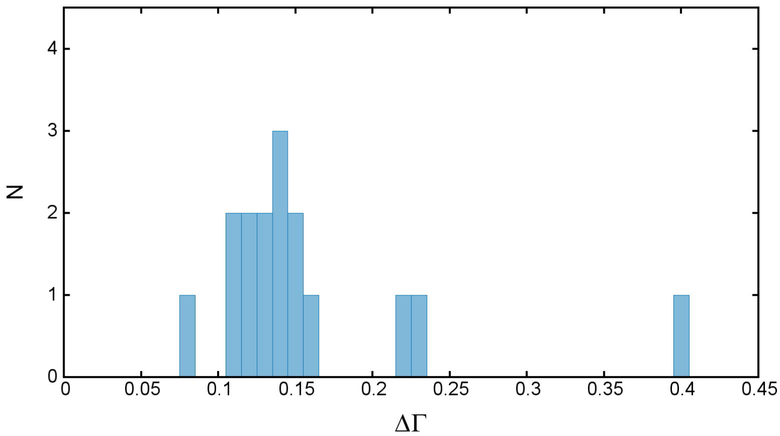

(a) Whole distribution of $\Delta\Gamma$

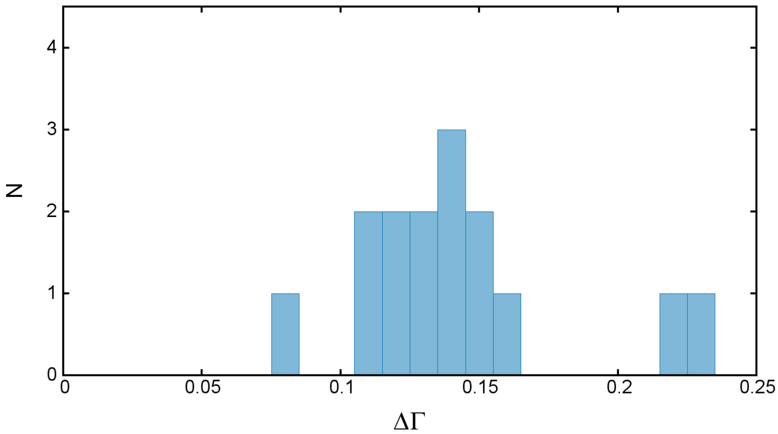

(b) Distribution of $\Delta\Gamma$ without Centaurus A

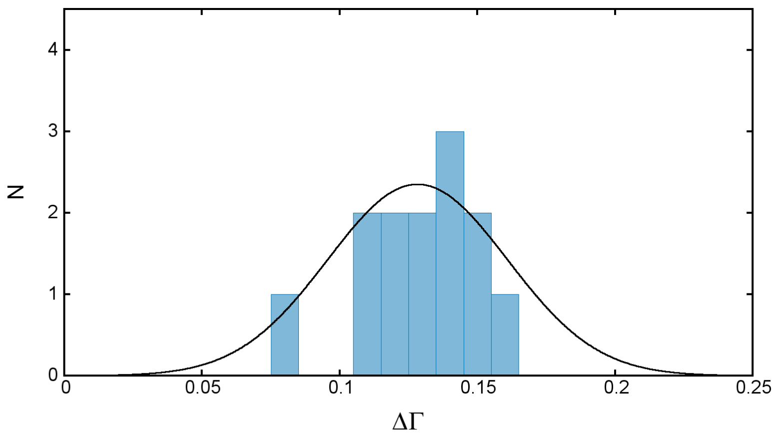

(c) Fitted gaussian curve over final distribuion (without Cen A, Mrk 915 and NGC 4593)

Figure 4.11: Distribution of $\Delta\Gamma$ for the FPMA detector

4.4 Comparison with other studies

So far only one cross-calibration analysis between *XMM-Newton* and *NuSTAR* was published (Madsen et al., 2017a). They performed a full analysis of the cross-normalisation constants between the satellites *Chandra*, *NuSTAR*, *Swift*, *Suzaku*, and *XMM-Newton* for 3C 273 and

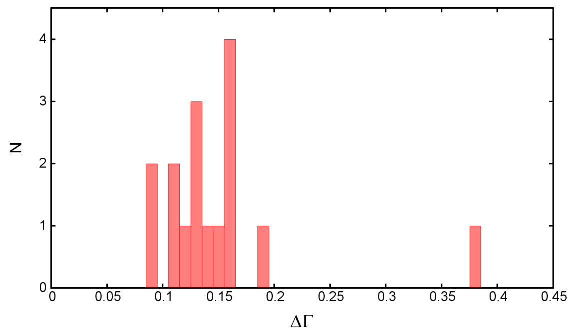

(a) Whole distribution of ΔΓ

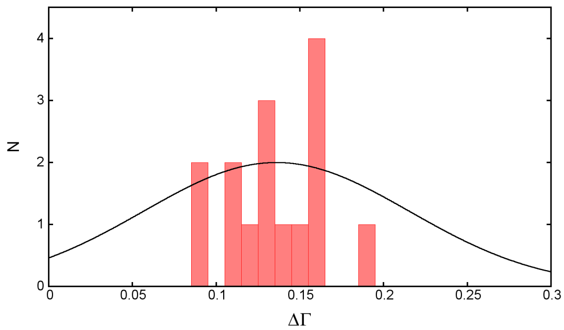

(b) Fitted gaussian curve over final distribution (without Cen A)

Figure 4.12: Distribution of ΔΓ for the FPMB detector

Parameter	Instruments	This work	Madsen et al. (2017a)[2]
c	EPIC-pn/FPMA	1.05 ± 0.01	1.11 ± 0.03
	EPIC-pn/FPMB	1.09 ± 0.02	1.16 ± 0.02
$\Delta\Gamma$	EPIC-pn/FPMA	0.13 ± 0.03	0.10 ± 0.09
	EPIC-pn/FPMB	0.16 ± 0.03	0.01 ± 0.09

Table 4.8: Comparison of c and $\Delta\Gamma$ with Madsen et al. for 3C 273.

PKS 2155-304. Since 3C 273 was in the sample that we analysed, we can compare their and our results directly. They used a simple power-law and `tbabs` for absorption, very similar to our model for 3C 273 (see Table 4.3). However, they used a fitting range from 3 to 7 keV, while we used all data between 3 and 10 keV. Another difference lies in the data extraction for which we used SAS version 15.0.0 and Madsen et al. SAS version 14.0.0. The values of c and $\Delta\Gamma$ are given in Table 4.8. Although they did not include a power-law index comparison in the paper, they showed the values for Γ, being derived in individual fits, which we used for calculating the correspondent $\Delta\Gamma$. While the difference in the power-law slope matches for the FPMA detector, there is nearly no difference between the FPMB detector and EPIC-pn according to Madsen et al. (2017a). Additionally the cross-normalisation constants between the EPIC-pn and the FPM detectors found by Madsen et al. (2017a) are much larger than the values found in this work.

4.5 Outlook

Further studies are necessary for the progress of improving the cross-calibration between *XMM-Newton* and *NuSTAR*, since we could see that there can be quite different results even for the same source. The difference of $\Delta\Gamma \propto 0.1$ in the power-law slopes is found to be consistent over all the sources and observations, regardless of the model. An explanation can be a principal, energy dependent mis-calibration in either one or both of the instruments.
The cross-normalisation constant c reveals differences in the flux normalisations of both satellites and shows some variations for which the origin has yet to be determined.
Recently there was an observation of the Crab nebula by *NuSTAR* without its mirrors (Madsen et al., 2017b). They find the true intrinsic flux to be 12% higher than the flux measured in an observation that includes the *NuSTAR* optics. Observing the stray light from the Crab allowed

[2] Since c and $\Delta\Gamma$ were not given directly in the paper, we calculated c from the flux values and $\Delta\Gamma$ from the given power-law slopes.

Madsen et al. (2017b) to measure new detector absorption parameters, which resulted in an update of the detector absorption files in CALDB20160606.
The surveys of AGN and other astrophysical sources depend on the cooperation of different satellites, because radiation processes, e.g., synchrotron radiation, exist in broad spectral ranges, which can only be studied by many different instruments working together.

Bibliography

Aartsen, M. G., Abbasi, R., Abdou, Y., et al. 2013, Physical Review Letters, 111, 021103

Abdo, A. A., Ackermann, M., Ajello, M., et al. 2011, ApJ, 736, 131

Antonucci, R. 1993, ARA&A, 31, 473

Antonucci, R. R. J. 1984, ApJ, 281, 112

Antonucci, R. R. J. & Miller, J. S. 1985, ApJ, 297, 621

Baade, W. & Minkowski, R. 1954, ApJ, 119, 206

Balbus, S. A. & Hawley, J. F. 1991, ApJ, 376, 214

Baldwin, J. A., Ferland, G. J., Korista, K. T., Hamann, F., & Dietrich, M. 2003, ApJ, 582, 590

Barthel, P. 1989a, Scientific American, 260, 20

Barthel, P. D. 1989b, ApJ, 336, 606

Beckmann, V. & Shrader, C. 2012, Active Galactic Nuclei (Wiley-VCH Verlag GmbH and Co. KGaA)

Bendo, G. J. & Joseph, R. D. 2004, AJ, 127, 3338

Bennett, A. S. 1962, MemRAS, 68, 163

Blandford, R. D. & Payne, D. G. 1982, MNRAS, 199, 883

Blandford, R. D. & Znajek, R. L. 1977, MNRAS, 179, 433

Blumenthal, G. R. & Gould, R. J. 1970, Reviews of Modern Physics, 42, 237

Bolton, J. G., Gardner, F. F., & Mackey, M. B. 1964, Australian Journal of Physics, 17, 340

Böttcher, M., Reimer, A., Sweeney, K., & Prakash, A. 2013, ApJ, 768, 54

Brenneman, L. W., Reynolds, C. S., Wilms, J., & Kaiser, M. E. 2007, ApJ, 666, 817

Bridle, A. H., Hough, D. H., Lonsdale, C. J., Burns, J. O., & Laing, R. A. 1994, AJ, 108, 766

Brinkmann, W., Siebert, J., Kollgaard, R. I., & Thomas, H.-C. 1996, A&A, 313, 356

Celotti, A., Padovani, P., & Ghisellini, G. 1997, MNRAS, 286, 415

Cohen, M. H., Cannon, W., Purcell, G. H., et al. 1971, ApJ, 170, 207

Corbin, M. R. 1995, ApJ, 447, 496

Curtis, H. D. 1918, Publications of Lick Observatory, 13, 9

Davidson, K. & Netzer, H. 1979, Reviews of Modern Physics, 51, 715

Day, G. A., Shimmins, A. J., Ekers, R. D., & Cole, D. J. 1966, Australian Journal of Physics, 19, 35

Dermer, C. D., Schlickeiser, R., & Mastichiadis, A. 1992, A&A, 256, L27

Doeleman, S. S., Fish, V. L., Schenck, D. E., et al. 2012, Science, 338, 355

Edge, D. O., Shakeshaft, J. R., McAdam, W. B., Baldwin, J. E., & Archer, S. 1959, MemRAS, 68, 37

Fanaroff, B. L. & Riley, J. M. 1974, MNRAS, 167, 31P

Fath, E. A. 1909, Lick Observatory Bulletin, 5, 71

Fürst, F., Müller, C., Madsen, K. K., et al. 2016, ApJ, 819, 150

García, J., Dauser, T., Lohfink, A., et al. 2014, ApJ, 782, 76

Ghisellini, G., Della Ceca, R., Volonteri, M., et al. 2010, MNRAS, 405, 387

Ghisellini, G. & Madau, P. 1996, MNRAS, 280, 67

Ghisellini, G., Maraschi, L., & Treves, A. 1985, A&A, 146, 204

Harrison, F. A., Craig, W. W., Christensen, F. E., et al. 2013, ApJ, 770, 103

Heckman, T. M. 1980, A&A, 87, 152

Ho, L. C., Filippenko, A. V., & Sargent, W. L. W. 1993, ApJ, 417, 63

Ho, L. C., Filippenko, A. V., & Sargent, W. L. W. 1997, ApJ, 487, 568

Hoffmeister, C. 1929, Astronomische Nachrichten, 236, 233

Hogg, D. E., MacDonald, G. H., Conway, R. G., & Wade, C. M. 1969, AJ, 74, 1206

Hoyle, F. & Fowler, W. A. 1963, MNRAS, 125, 169

Hubble, E. P. 1926, ApJ, 64

Jansen, F., Lumb, D., Altieri, B., et al. 2001, A&A, 365, L1

Kellermann, K. I., Condon, J. J., Kimball, A. E., Perley, R. A., & Željko Ivezić. 2016, The Astrophysical Journal, 831, 168

Kellermann, K. I., Sramek, R., Schmidt, M., Shaffer, D. B., & Green, R. 1989, AJ, 98, 1195

Kerr, R. P. 1963, Physical Review Letters, 11, 237

Khachikian, E. Y. & Weedman, D. W. 1974, ApJ, 192, 581

Kigure, H. & Shibata, K. 2005, ApJ, 634, 879

Krauß, F., Kadler, M., Mannheim, K., et al. 2014, A&A, 566, L7

Krauß, F., Wang, B., Baxter, C., et al. 2015, ArXiv e-prints

Krauß, F., Wilms, J., Kadler, M., et al. 2016, A&A, 591, A130

Laing, R. A. & Bridle, A. H. 1987, MNRAS, 228, 557

Lang, K. R. 1999, Astrophysical Formulae, Vol. 1 (Springer Verlag)

Lasota, J.-P., Abramowicz, M. A., Chen, X., et al. 1996, ApJ, 462, 142

Leavitt, H. S. & Pickering, E. C. 1912, HCOC, 173, 1

Lohfink, A. M., Reynolds, C. S., Jorstad, S. G., et al. 2013, ApJ, 772, 83

Lohfink, A. M., Reynolds, C. S., Miller, J. M., et al. 2012, ApJ, 758, 67

Lucchini, M., Tavecchio, F., & Ghisellini, G. 2017, MNRAS, 466, 4299

Madsen, K. K., Beardmore, A. P., Forster, K., et al. 2017a, AJ, 153, 2

Madsen, K. K., Forster, K., Grefenstette, B. W., Harrison, F. A., & Stern, D. 2017b, ApJ, 841, 56

Madsen, K. K., Fürst, F., Walton, D. J., et al. 2015, ApJ, 812, 14

Mannheim, K. 1993a, PhRvD, 48, 2408

Mannheim, K. 1993b, A&A, 269, 67

Mannheim, K. 1995, Astroparticle Physics, 3, 295

Mannheim, K. & Biermann, P. L. 1989, A&A, 221, 211

Mannheim, K. & Biermann, P. L. 1992, A&A, 253, L21

Maraschi, L., Ghisellini, G., & Celotti, A. 1992, ApJL, 397, L5

Marinucci, A., Matt, G., Kara, E., et al. 2014, MNRAS, 440, 2347

Martí-Vidal, I., Muller, S., Vlemmings, W., Horellou, C., & Aalto, S. 2015, Science, 348, 311

Matt, G., Marinucci, A., Guainazzi, M., et al. 2014, MNRAS, 439, 3016

Matthews, T. A. & Sandage, A. R. 1963, ApJ, 138, 30

McKinney, J. C. 2006, MNRAS, 368, 1561

McKinney, J. C., Tchekhovskoy, A., Sadowski, A., & Narayan, R. 2014, MNRAS, 441, 3177

Mortlock, D., Warren, S., Patel, M., et al. 2011, in Galaxy Formation, 88

Osterbrock, D. E. 1989, Astrophysics of gaseous nebulae and active galactic nuclei

Osterbrock, D. E. & Koski, A. T. 1976, MNRAS, 176, 61P

Osterbrock, D. E. & Martel, A. 1993, ApJ, 414, 552

Pacholczyk, A. G. 1970, Radio Astrophysics (W. H. Freeman and Company)

Padmanabhan, T. 2000, Theoretical Astrophysics, Vol. 1 (Cambridge University Press)

Parker, M. L., Komossa, S., Kollatschny, W., et al. 2016, MNRAS, 461, 1927

Penrose, R. 1969, Nuovo Cimento Rivista Serie, 1

Price, R. M. & Milne, D. K. 1965, Australian Journal of Physics, 18, 329

Pringle, J. E. 1981, ARA&A, 19, 137

Richards, G. T., Strauss, M. A., Fan, X., et al. 2006, AJ, 131, 2766

Rybicki, G. B. & Lightman, A. P. 1979, Radiative Processes in Astrophysics (John Wiley and Sons, Inc.)

Salpeter, E. E. 1964, ApJ, 140, 796

Scarpa, R. & Falomo, R. 1997, A&A, 325, 109

Scheuer, P. A. G. & Readhead, A. C. S. 1979, Nature, 277, 182

Schmidt, M. 1963, Nature, 197, 1040

Severgnini, P., Ballo, L., Braito, V., et al. 2015, MNRAS, 453, 3611

Seyfert, C. K. 1943, ApJ, 97, 28

Shakura, N. I. & Sunyaev, R. A. 1973, A&A, 24, 337

Shields, J. C. 1992, ApJL, 399, L27

Sikora, M., Begelman, M. C., & Rees, M. J. 1994, ApJ, 421, 153

Smith, M. G. 1975, ApJ, 202, 591

Smith, P. S., Schmidt, G. D., Jannuzi, B. T., & Elston, R. 1994, ApJ, 426, 535

Stuhlinger, M., Staubert, R., Wilms, J., Kreykenbohm, I., & Benlloch-García, S. 2004, MemSAI, 75, 527

Tavecchio, F., Maraschi, L., Sambruna, R. M., & Urry, C. M. 2000, ApJL, 544, L23

Terlevich, R. & Melnick, J. 1985, MNRAS, 213, 841

Ulrich, M.-H., Maraschi, L., & Urry, C. M. 1997, ARA&A, 35, 445

Urry, C. M. & Padovani, P. 1995, PASP, 107, 803

Vanden Berk, D. E., Richards, G. T., Bauer, A., et al. 2001, AJ, 122, 549

Verner, D. A., Ferland, G. J., Korista, K. T., & Yakovlev, D. G. 1996, ApJ, 465, 487

Weedman, D. W. 1977, ARA&A, 15, 69

Westfold, K. C. 1959, ApJ, 130, 241

Whitney, A. R., Shapiro, I. I., Rogers, A. E. E., et al. 1971, Science, 173, 225

Wilms, J., Allen, A., & McCray, R. 2000, ApJ, 542, 914

Wilms, J. & Kreykenbohm, I. 2015, Active Galactic Nuclei, Lecture, Lecture notes available at http://hydrus.sternwarte.uni-erlangen.de/~wilms/teach/agn1516/chapter0001.html

Wilms, J., Reynolds, C. S., Begelman, M. C., et al. 2001, MNRAS, 328, L27

Woltjer, L. 1959, ApJ, 130, 38

York, D. G., Adelman, J., Anderson, Jr., J. E., et al. 2000, AJ, 120, 1579

Zamorani, G., Henry, J. P., Maccacaro, T., et al. 1981, ApJ, 245, 357

Zel'dovich, Y. B. & Novikov, I. D. 1964, Soviet Physics Doklady, 9, 246

Acknowledgements

First and foremost I want to thank my supervisor Prof. Dr. Joern Wilms for his support, encouragement and advice. I am very grateful for the opportunity to attend the AGN conference 2016 at Garching, the IBWS conference 2017 at Karlsbad and Prof. Wilms' support for my traineeship at ESAC, whose project became part of this thesis.
I deeply want to thank Norbert Schartel and Maria Santos-Lleo for the wonderful and interesting time I had while working at ESAC. In addition, I want to thank all the trainees, who made the five months in Madrid so much fun, especially Alessandra, Kjell, Harry, Aleksi and Vedad.
Then, of course, I am very grateful to be part of the Remeis community, without which the Remeis observatory would not be such a welcoming and pleasent working place. Sincere thanks are given to all the Remeisen. I want to thank Matthias Kühnel and Ralf Ballhausen for their help with the *NuSTAR* data extraction and give a big thank you to Thomas Dauser, Sebastian Falkner and Javier García for their help during the preparation of my first conference talk. At this point I also want thank my office mates for hilarious conversations and apologise for my over-use of the word "Bieberkacke". I am looking forward to many years more of Remeis skiing and overturning during the annual canoeing, as well as (spontaneous) barbecues and pool parties.
Somehow, public outreach became important to me during the last year, probably also because of Simon Kreuzer. I am very grateful that he suggested to give a lecture about multiwavelength astronomy together at a "Schülerakademie", because it was a great experience and a lot of fun.
A big thank you to Basti, Tommy and Tobi for improving my thesis through helpful comments and fancy plot ideas.
Last but not least I want to thank my family and friends for their support.

This thesis has made use of ISIS functions (ISISscripts) provided by ECAP/Remeis observatory and MIT (http://www.sternwarte.uni-erlangen.de/isis/). In this thesis I use observations obtained with XMM-Newton, an ESA science mission with instruments and contributions directly funded by ESA Member States and the USA, NASA, as well as data from the NuSTAR mission, a project led by the California Institute of Technology, managed by the Jet Propulsion Laboratory, and funded by NASA. This work has made use of the NuSTAR Data Analysis Software (NuSTARDAS) jointly developed by the ASI Science Data Center and the California Institute of Technology.